A Device Characterization and Circuit Design Procedure for Realizing High-Power Millimeter-Wave IMPATT-Diode Amplifiers

DEAN F. PETERSON

Abstract—**A measurement and characterization technique is presented which allows design and realization of IMPATT amplifiers operating at maximum generation efficiency. Diodes mounted in a stable reduced-height waveguide circuit are characterized by their complex reciprocal scattering coefficient as a function of frequency, dc bias, and RF drive power level. In particular, terminal conditions which correspond to a maximum power exchange between the active one-port network and the source are identified and then used to design and realize controlled-gain maximum generation-efficiency amplifiers. Simple equalization networks are shown to provide a wide range of available amplifier gains between limits set by stability requirements. As an example, the technique is effectively used with silicon diodes at K_a-band (33–40 GHz) to realize a 7-dB gain 250-mW power amplifier with 5-GHz bandwidth.**

I. Introduction

IMPATT diodes are now very widely used and are often a preferable source for millimeter-wave power generation. Their small size and solid-state advantages have made them an attractive microwave power source in many commercial and military systems for a variety of applications.

One promising application is the use of these devices as amplifiers which are saturated with respect to their available *added* power and therefore always operate at maximum generation efficiency. This application becomes even more promising if a degree of amplifier gain flexibility exists and can be realized by design while generation efficiency remains maximum. In this paper we present a device characterization and circuit design procedure which has allowed the realization of maximum generation efficiency millimeter-wave IMPATT-diode amplifiers which have power gain flexibility. The amplifier generation efficiency is also equivalent to the oscillator efficiency of the devices.

The diodes mounted in a reduced-height waveguide circuit are characterized by their complex scattering coefficient as a function of frequency, dc input power (bias), and RF drive power level. The scattering coefficient at which the circuit adds maximum power and the corresponding drive level are identified at any given dc bias. Equalization networks which preserve system stability are then determined for the circuit which allows amplifiers to be constructed having a specified gain with the overall generation efficiency remaining constant at maximum. An example of the technique is presented graphically, demonstrating the realization of a 5-GHz-wide amplifier with 250-mW output, 7-dB power gain, and 3.92 percent generation efficiency.

Manuscript received January 11, 1973; revised March 7, 1973. This work was sponsored by the Department of the Air Force.

The author is with the Massachusetts Institute of Technology, Lincoln Laboratory, Lexington, Mass. 02173.

II. Approach Taken for Characterizing IMPATT Diodes for Use as Amplifiers

A. Definition of the Active Device for Experimental Characterization

An IMPATT diode is a two-terminal negative resistance device whose linear and nonlinear properties are generally well understood and have been treated extensively both theoretically and experimentally [1]–[5]. Unfortunately, the terminals of this active device as normally defined are not usually accessible for *direct* diode measurement and characterization, and amplifier design beginning at these terminals is rarely possible. Although some diode properties can often be obtained by de-embedding, the parasitic elements immediately surrounding the diode (e.g., package parameters) are usually difficult to control in the deterministic manner required for construction of stable well-designed amplifiers.

In this paper, we require direct characterization by measurement of the "active device," thereby necessitating an environment for the IMPATT diode which will provide terminals which are compatible with existing microwave measurement equipment. These interfacing terminals define our active device; its properties appropriate for amplifier design will be determined by measurement only. This approach results in a generalized coupling network or embedding network existing between the actual diode and the external measurement terminals which can degrade the fundamental performance limitations of the IMPATT. Constraints on this embedding network necessary for this approach to be useful for amplifier design will be discussed further.

B. Network Terminal Description

The most fundamental and direct measurement of a one-port network at microwave frequencies is the network reflection coefficient in a transmission line or waveguide environment. As this description is also most appropriate for reflection amplifiers, we shall use the wave variable approach for describing the active one-port containing the IMPATT diode. With reference to Fig. 1, the incident wave (excitation) $a_d(t)$ is given by

$$a_d(t) = A_d e^{j\omega t} + \text{c.c.} \tag{1}$$

where A_d has dimensions of $\sqrt{\text{power}}$ and $|A_d|^2$ is the power carried in the incident wave. Because the active one-port is

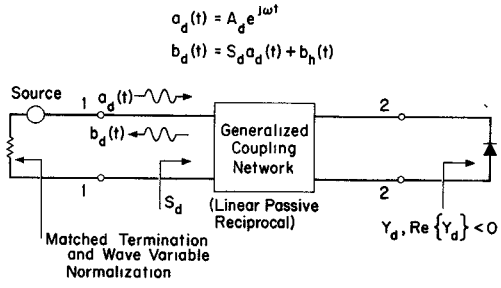

Fig. 1. Generalized embedding of an IMPATT diode required for direct measurement and characterization at terminals 1–1.

generally nonlinear, the reflected wave response to (1) $b_d(t)$ is normally[1]

$$b_d(t) = B_d e^{j\omega t} + \sum_{n=2}^{\infty} B_{dn} e^{jn\omega t} + \text{c.c.} \tag{2}$$

$$= s_d(\omega, |A_d|) A_d e^{j\omega t} + \text{c.c.} + b_h(t) \tag{3}$$

where s_d is the complex scattering coefficient at the fundamental normalized to a matched termination in the waveguide or transmission-line measurement system, and $b_h(t)$ is the sum of all the reflected waves at the harmonics. In this paper we shall not attempt to determine and characterize the response $b_h(t)$, and harmonic effects on amplifier performance are generally neglected. This is not to say that proper harmonic control cannot improve IMPATT performance (efficiency, bandwidth, etc.) as 3–5-dB variations in oscillator and amplifier output power can occur with second-harmonic tuning [6]–[10]. Although these effects have been observed, specification of optimum harmonic terminations is not presently possible, and for this reason $b_h(t)$ is not considered in (3). It is possible to make $b_h(t) = 0$ by lossless low-pass filtering in the embedding network but the resulting harmonic terminations for the diode are not necessarily optimum.

We thus describe the one-port by the nonlinear single-frequency response function $s_d(\omega, |A_d|)$, where

$$B_d = s_d(\omega, |A_d|) A_d \tag{4}$$

and $|B_d|^2$ is the reflected power at ω. The network is then active whenever $|s_d| > 1$ since $|B_d|^2 > |A_d|^2$ and RF power is being generated through dc to RF conversion.

The generation efficiency η_g of the network is defined as

$$\eta_g = \frac{P_{gd}}{P_D} \tag{5}$$

where P_{gd} is the net added power from the network given by

$$P_{gd} = |B_d|^2 - |A_d|^2 = [|s_d(|A_d|)|^2 - 1]|A_d|^2 \tag{6}$$

and P_D is the dc power supplied to the diode. In our characterization, we find that a value for $|A_d| = |A_{d0}|$ exists such that P_{gd} is a maximum P_{gm}. The value of $s_d(|A_{d0}|)$ will be referred to as s_{d0}. This information is used in Section IV to design amplifiers which operate at maximum generation efficiency for the given embedding network.

We shall find in Section III that the network is most appropriately characterized by its inverse scattering coefficient s_r as a function of *incident power* $|A_d|^2$, i.e.,

$$s_r = s_r(\omega, |A_d|) = \frac{1}{s_d(\omega, |A_d|)} \tag{7}$$

as this allows one to work inside the unit circle in the complex plane, and incident power is easily monitored.

C. Properties of the IMPATT-Diode Embedding Network

The coupling network that necessarily exists between the diode and the accessible terminals can degrade the fundamental performance limitations of the IMPATT diode. Therefore, in order for our approach to amplifier design to have merit, the embedding network should have some general properties which tend to minimize such degradations and allow useful design.

Ideally the embedding network should be lossless and have no transmission zeros in the frequency range where the *diode* is active, i.e., if the diode has an admittance Y_d, then from Fig. 1 $|s_d| > 1$ whenever Re $\{Y_d\} < 0$. Because of the diode series resistance and other circuit loss, the lossless condition is not possible and the net power crossing port 1, P_{gd}, will be less than the power generated by or available from the active diode. The loss structure of the network should thus be arranged to minimize this power loss. The presence of lossless parasitic energy storage elements can also reduce the inherent gain-bandwidth limitation of the diode, and excess energy storage should be minimized so that broad-band equalization can be achieved.

Finally, since the network terminal behavior must be measureable, the system must be stable under measurement conditions, i.e., when port 1 is terminated in its reference (a matched load) there are no source-free oscillations in the system. This condition can be nontrivial to establish since stability can only be defined from a knowledge of the diode admittance which in turn can only be determined by de-embedding which requires a stable system for measurement.

Generally, the development of the appropriate embedding network initially requires reasonable assumptions about the diode characteristics in addition to a well-controlled adjustable circuit.

III. Measurement and Characterization of Active Mounted Diodes

A. Millimeter-Wave Embedding Network

For our 40-GHz amplifiers, a waveguide mounting structure was appropriate for compatibility with existing measurement equipment and is shown in Fig. 2. This configuration is quite standard for waveguide mounting of many active devices (varactors, Gunn, and IMPATT diodes) and it obeyed the general network properties specified above for the class of millimeter-wave IMPATTs used in our amplifiers.

The packaged diode is mounted to a copper stud which makes intimate contact with the circuit to provide good heat sinking. Bias is supplied to the diode through a special low-pass coaxial filter which must have the following properties: 1) provide isolation between the bias supply and the diode in-band; 2) present a low loss to the packaged diode to minimize power loss in the mount; and 3) have a controllable reactance to help establish circuit stability and gain characteristics. Such a filter was realized by three sections of coaxial line terminated in a tapered section of absorbing material which provided a *known* reference impedance (50 Ω) to allow deterministic design of the filter. The absorbing material also

[1] We do not include frequency components that may arise from parametric instabilities or subharmonic generation [10], [11], as these are considered deleterious to amplifier performance and should not be present in correctly designed amplifiers.

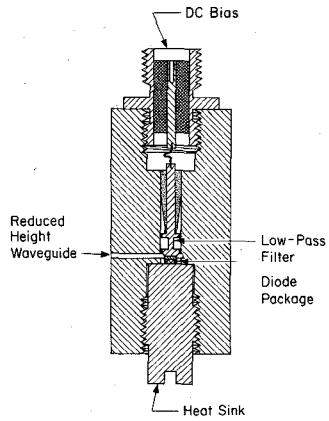

Fig. 2. A millimeter-wave reduced-height waveguide mount for characterizing K_a-band IMPATT diodes.

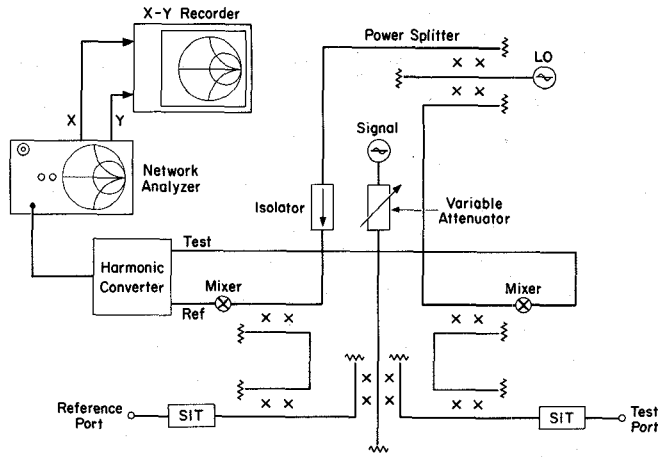

Fig. 3. Frequency-translated network analyzer used for measuring active IMPATT networks.

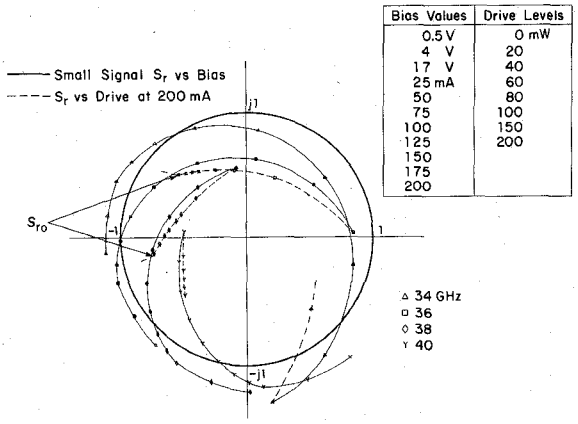

Bias Values	Drive Levels
0.5 V	0 mW
4 V	20
17 V	40
25 mA	60
50	80
75	100
100	150
125	200
150	
175	
200	

Fig. 4. Single-frequency inverse scattering coefficient of mounted K_a-band IMPATT diodes as a function of dc bias and RF drive power.

results in isolation between the diode and the outside world. The input impedance of this filter was usually between 0.5–1-Ω resistance in-band with a capacitive reactance which could be varied appropriately by design to establish stability. The waveguide was standard K_a-band (WR28) reduced in height from 0.140 to 0.020 in (approximately the package height) to reduce excess energy storage around the post contacting the diode and provide a lower "impedance" level for the waveguide. Stability was achieved by adjusting the input reactance of the bias filter and the position of the waveguide backshort under matched loading on the reduced-height waveguide port. This basic circuit was duplicated many times, being fabricated to tight tolerances and good surface finish quality by the electroforming technique. This unit was considered the active device, where the measurement terminals are represented by reduced-height waveguide with a reference plane at the face of the mount.

B. Measurement System

The active one-ports were characterized by their input reflection coefficient as measured in the reduced-height waveguide of the mount. This reflection coefficient is equivalent to the scattering coefficient s_d (4) of the network normalized to a matched termination in the reduced-height waveguide. A "characteristic impedance" for this termination and the waveguide can be chosen arbitrarily (1 Ω, for example) if an equivalent impedance description of the one-port is desired.

The method of measuring s_d was to use the network analyzer-reflectometer system shown in Fig. 3. This system normally measures the reflection coefficient normalized to standard K_a-band (WR28) waveguide, and measuring s_d required a pair of matched broad-band stepped impedance transformers (SIT) from 0.140×0.280 in to 0.020×0.280 in for use on both the reference and test ports. These transformers were symmetrical seven-section maximally flat types made by electroforming and they provided the required matched transformation (>30-dB return loss, <0.1-dB insertion loss from 33 to 40 GHz) to the reduced-height waveguide of the mount.

In normal operation this system measures s_d of a network on the test port with a short-circuit reference. With active networks in which $|s_d| > 1$ this necessitates working outside the unit circle or normal Smith chart in the complex plane. If the reference and test ports are interchanged, the system now measures the short relative to a reference s_d and $s_r \triangleq (1/s_d)$ is displayed and can be directly recorded. This allows one to work inside the unit circle for active one-ports, and in terms of a Smith chart display this transformation provides a direct readout of an equivalent normalized *negative* impedance. This kind of display also provides information for readily defining amplifier stability and gain characteristics as will be shown in Section IV.

C. Behavior of s_r for Silicon Diodes

We generally measure s_r at a fixed reference plane as a function of frequency, dc bias, and RF drive power level $|A_d|^2$ over the ranges of interest. This was generally accomplished at each of a set of frequencies by making small signal measurements versus bias from 0 V to breakdown and then to an avalanche current corresponding to a dc power limitation (usually thermal). At this maximum dc current or at the current established for amplifier operation, the RF drive power $|A_d|^2$ was increased from small signal and $s_r(|A_d|^2)$ was recorded. Normally, a point on this curve s_{r0} could readily be identified at which the added power P_{gd} was a maximum P_{gm} at $|A_d|^2 = |A_{d0}|^2$. This large signal measurement is in accordance with (4) and is single frequency because any higher harmonics generated and mixing with the network analyzer local oscillator are well out of the IF bandwidth of the mixer-harmonic converter.

A typical plot of single-frequency characteristics for silicon diodes is shown in Fig. 4 for several frequencies. Below breakdown between 0 V and breakdown V_B, the diode is passive

and $|s_r| > 1$. The values of $s_r(V)$ in this region were recorded to use as reference values for de-embedding purposes in accordance with that described in [12], the results of which give an indication of mounting circuit loss as well as the linear and nonlinear properties of the active diode region. The curve defined by $s_r(V)$ in this region is a portion of a circular arc as is normally the case with varactors. As avalanche current begins, the small-signal single-frequency s_r curve breaks into the region bounded by the extended varactor circle, thus indicating negative resistance exists at the terminals of the active diode region [12]. The value of $|s_r|$ is greater than unity for low avalanche currents because the diode series resistance and other circuit loss mask this negative resistance. Eventually a bias current is reached at which $|s_r| = 1$; further increase in bias results in $|s_r| < 1$ and the network is active and has net power gain.

If the measurement frequency is low enough and the bias current high enough, we can have $|s_r| > 1$, again indicating network or diode passivity. This is the effect of the avalanche frequency increasing with current and eventually equaling the measurement frequency [12]. Although the network may be passive at the operating current, power gain can often be achieved at high drive power as $|s_r| < 1$ is again possible. This effect has previously been observed in IMPATT amplifiers and is evident for the given characteristics at 34 GHz where the small signal gain is less than unity ($|s_r| > 1$) at 200 mA, but large signal gain becomes possible at 20–30-mW drive power. For this diode, 34 GHz is approximately the avalanche frequency at 200-mA bias current.

At 36, 37, and 38 GHz a distinct break in the $s_r(|A_d|^2)$ curve is observed. For this class of device, this breakpoint was almost always associated with maximum added power P_{gm}, and further drive would result in a rapid decrease in P_{gd}. The results of de-embedding [5], [12] showed that at P_{gm} the diode peak RF voltage was about 7.5 V for a diode operating at 25 V and 200 mA, or 30 percent of the dc voltage. This agrees with theory for single-drift silicon diodes [13].

The added power for the diode characterized in Fig. 4 is shown in Fig. 5 as a function of drive power $|A_d|^2$ at 37.5 GHz. For this diode, the added power has a distinct maximum of 220 mW at $|A_{d0}|^2 = 140$ mW and $P_d = 5.5$ W. The value of $|A_{d0}|$ and the shape of the curve $P_{gd}(|A_d|^2)$ are a function of device-circuit interaction and varied somewhat among the different silicon diodes examined.

The maximum generation efficiency η_{gm} as a function of P_D for the same diode is also shown in Fig. 5. This generation efficiency was determined by finding P_{gm} from measured curves of $P_{gd}(|A_d|^2)$ at several values of P_D. The diode is approaching 5 percent for η_{gm} at $P_D = 7$ W, but operation at this dc power would result in device temperatures around 300°C. At $P_D = 5$ W (200°C) the efficiency is nearly 4 percent.

Of the 100 diodes initially available, the behavior shown in Fig. 5 was typical of the best 15 percent, the remainder generally having smaller generation efficiencies (2 percent versus 4 percent) under similar dc conditions.

D. Summary

In this section, we have attempted to characterize IMPATT diodes in the manner presented in Section II for use in the design and construction of reflection amplifiers which operate at maximum generation efficiency. A technique was presented that allows mounted devices to be described by their inverse reflection coefficient as a function of frequency, bias, and RF drive power. It was observed that this two-terminal active network has a terminal condition which results in a maximum single-frequency power exchange between the network and the source. Our task is now to design amplifiers which have specified gain and bandwidth characteristics and operate at this maximum generation efficiency.

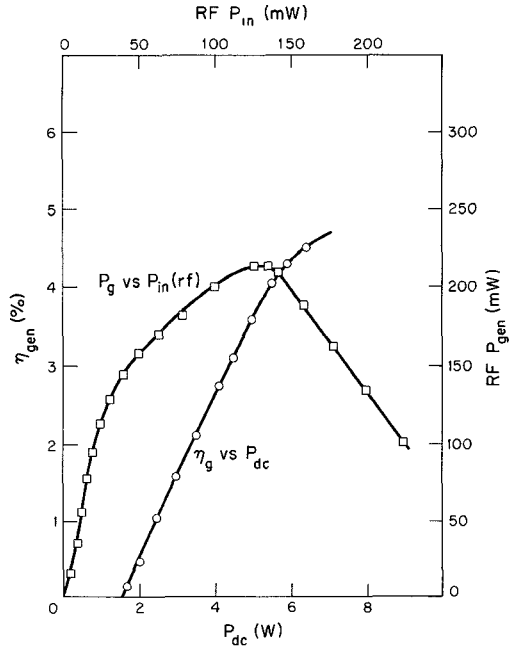

Fig. 5. Added power as a function of drive power at 5.5 W dc power and 37.5 GHz, and generation efficiency versus dc power for the same diode.

IV. Design of Optimum Generation-Efficiency Amplifiers Using Active Mounted IMPATT Diodes

A. General Reflection Amplifier Configuration

The general form of a reflection amplifier is shown in Fig. 6, where operation is described in terms of the wave variables and scattering parameters. The amplifier consists of three basic elements: a circulator to separate incident and reflected power; a lossless reciprocal two-port equalization network; and an active one-port which has a scattering coefficient greater than unity in magnitude. In this configuration, the normalization of the wave variables at port 2 of the equalization network must be the same as that for the active network, and likewise for the normalization at port 1 and the circulator. The normalization at port 1 and port 2 may be different, however. At present, we shall assume the circulator to be ideal, so that $s_c = 0$ and $|A_1| = |A_s|$ and $|B_l| = |B_1|$.

The active one-ports will be those defined and characterized in the previous sections; obviously these are easily made into unilateral two-port amplifiers with power gains of $|s_a|^2$ with an equalization network consisting of a transformer (e.g., SIT which matches between the normalizations of the circulator and active network). Usually, however, the gain characteristics of this amplifier are not the desired ones and more complex equalization is required.

For the amplifier of Fig. 6, the power gain is given by $|s_a|^2 > 1$, where in terms of the two-port s parameters

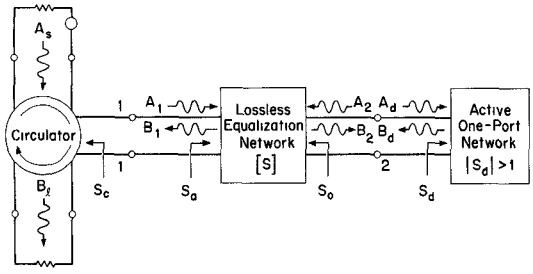

Fig. 6. General form of a reflection amplifier.

$$s_a = \frac{B_1}{A_1} = s_{11} + \frac{s_{12}^2}{\frac{1}{s_d} - s_{22}} = s_{11} + \frac{s_{12}^2}{s_r - s_{22}} \tag{8}$$

and the gain can be modified by proper control of the s parameters. In our case, we want the amplifier to operate at maximum generation efficiency at a value of power gain appropriate for a given system requirement. From Section III, we know the conditions $|A_{d0}|^2$ and s_{r0} such that the one-port generates maximum power P_{gm}. Since this added power is $|B_d|^2 - |A_d|^2 = |A_2|^2 - |B_2|^2$ and the added power of the amplifier P_{ga} is $|B_1|^2 - |A_1|^2$, then for a lossless equalization network we must have

$$|A_1|^2 + |A_2|^2 = |B_1|^2 + |B_2|^2 \tag{9}$$

or

$$P_{ga} = |B_1|^2 - |A_1|^2 = |A_2|^2 - |B_2|^2 = P_{gd}. \tag{10}$$

Thus, whenever $P_{gd} = P_{gm}$, $P_{ga} = P_{gm}$ and the added power and generation efficiency of the amplifier is equal to that of the active network. Note that (9) and (10) are independent of the gain $|s_a|^2$ of the amplifier. If the amplifier is to operate at maximum generation efficiency then there is a required relationship between amplifier gain $|s_a|^2$, amplifier input power $|A_s|^2$, and maximum added power P_{gm} given by

$$\{|s_a|^2 - 1\}|A_s|^2 = P_{gm} = \text{const} \tag{11}$$

and operation under this condition establishes the optimum conditions at the terminals of the active one-port. In terms of a required amplifier output power $P_0 > P_{gm}$, the equivalent relation to (11) implies a gain

$$|s_a|^2 = \frac{P_o}{P_i} = \frac{P_o}{P_o - P_{gm}} \tag{12}$$

where P_i is the amplifier input power $|A_s|^2$.

The tradeoffs implied in (11) and (12) are presented graphically in Fig. 7, which shows P_o/P_{gm} and P_i/P_{gm} as a function of the amplifier gain $|s_a|^2$. Note that the higher the output power, the lower the gain and vice versa, and this will be a design decision.

Our task now is to determine the scattering parameters of the equalization network in conjunction with the active network in order to realize any desired value of $|s_a|^2$ at $P_{ga} = P_{gm}$. We shall see that not all values for gain are available because of constraints imposed on the equalizer by stability requirements.

A word should be mentioned at this point about the validity of (11) as it is the basis of our large signal design. This equation is strictly valid for linear circuits but we are in reality dealing with a nonlinear element which may have significant harmonic content under the conditions which maximize added power. One may consider (11) valid if either or both of the following conditions exist: 1) the addition of the equalization network does not appreciably modify the harmonic terminations of the diode; and 2) changes in harmonic terminations do not have a significant effect on generation efficiency.

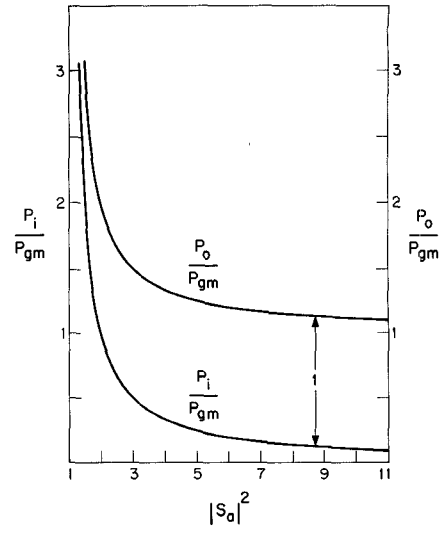

Fig. 7. The tradeoffs between amplifier gain $|s_a|^2$ and input and output power required for operation at maximum generation efficiency.

We show in Section V that simple but effective equalization networks do not result in significant modification of generation efficiency.

B. Stability

There are constraints on the s parameters of the equalization network imposed by requiring the amplifier to remain stable. The definition of stability used in this paper is that normally identified with linear circuits, i.e., no source-free oscillations are present in the system. For our case this definition is valid only for incremental signal analysis as only under this condition does the active network behave in a truly linear fashion. Since oscillations build up from noise which can be considered an incremental signal, stability analysis in the small signal case can determine the conditions under which the noise can reinforceably build into an oscillation. Thus system stability as we require can be analyzed from small signal data, in particular small signal $s_r(\omega)$ for the active network. Although this definition of stability is useful, it has no value in determining large signal instabilities, such as parametric instabilities, which can occur in IMPATT-diode networks (11). No such instabilities were observed in the amplifiers described here.

Stability as defined above can easily be determined for the equalized amplifier configuration shown in Fig. 6. The amplifier will be unstable if there are any poles of s_a in the right half plane (RHP) of complex frequencies. From (8), it is clear that since s_d has no RHP poles (it was measurable), poles of s_a in the RHP can only arise from zeros of $1/s_d - s_{22}$ or $1 - s_d s_{22}$ in the RHP. Thus the stability can be inves-

tigated in the same manner as for an amplifier with open loop gain $s_d(\omega)$, $|s_d(\omega)| > 1$ and feedback $s_{22}(\omega)$, $|s_{22}(\omega)| < 1$. Using Nyquist's criteria one can easily show that if

$$|s_{22}(\omega_0)| \geq \frac{1}{|s_d(\omega_0)|} = |s_r(\omega_0)| \tag{13a}$$

when

$$\arg s_{22}(\omega_0) = \arg \frac{1}{s_d(\omega_0)} = \arg s_r(\omega_0) \tag{13b}$$

for any frequency ω_0 then the system will probably be unstable. Exceptions can occur if more than one solution to (13) exists. As a *net* clockwise encirclement of $+1$ made by the vector $s_d(\omega)s_{22}(\omega)$ in the complex plane with increasing frequency may not occur, further investigation may be required. A solution to (13) is necessary but may not be sufficient for an oscillation to occur.

A solution to (13) is easily determined for any equalization network by comparing its $s_{22}(\omega)$ with the $s_r(\omega)$ of the active network determined by measurement. Although this stability determination is strictly valid only for small signal s_r, we shall insist on $s_{22}(\omega)$ functions which do not satisfy (13) for the large signal values of s_r used to characterize the diode at various drive levels. It is possible that an oscillator with output power P_{gm} could be built by having $s_{22} = s_{r0}$ at ω_0 even though (13) was not satisfied at any frequency for small signal $s_r(\omega)$, and we have observed this effect in the laboratory.

C. Specification of s Parameters for Desired Amplifier Gain

Having determined conditions on s_{22} for amplifier stability, we now wish to specify values for the s parameters which give the desired gain for the amplifier. By using the unitary properties of the the scattering parameters for the lossless two-port, we have $|s_{11}| = |s_{22}|$ and $|s_{12}|^2 = 1 - |s_{22}|^2$, and from (8) we may write

$$|s_a| = \left| \frac{1 - s_r s_{22}^*}{s_r - s_{22}} \right| \tag{14}$$

where $s_r = s_r(\omega, |A_d|^2)$. For a constant $|s_a|$ and a given value of s_r then (14) is the equation of a circle in the s_{22} plane with center C at

$$C = \frac{|s_a|^2 - 1}{|s_a|^2 - |s_r|^2} s_r \tag{15a}$$

and radius

$$R = \frac{1 - |s_r|^2}{|s_a|^2 - |s_r|^2} |s_a| . \tag{15b}$$

In Fig. 8 we have shown some constant $|s_a|$ circles for an arbitrary value of s_r. Note that all the circle centers lie on a line through the origin and the point s_r as can be seen from (15a). Thus any value of s_{22} on one of these circles will yield the same amplifier gain, although some of these values are not stable solutions. An amplifier with specified gain $|s_a(\omega)|$ can be realized if an $s_{22}(\omega)$ can be realized such that for each ω over the band of interest s_{22} lies on each corresponding $|s_a(\omega)|$ circle determined from (15) and $s_r(\omega)$. Such a function may not be realizable or very difficult to realize, and it must also represent a stable solution.

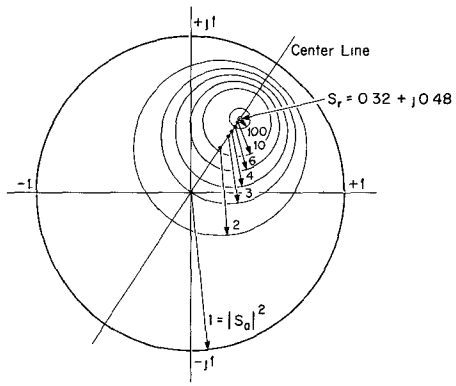

Fig. 8. Circular loci of s_{22} in the complex plane for constant amplifier power gain with a given s_r of $0.32 + j0.48$.

Since we are primarily interested in maximum generation-efficiency amplifiers, we set $s_r = s_{r0}$ in (14) and (15). Then if the desired amplifier power gain is $|s_a|^2$, an s_{22} for optimum performance is determined from (14) or (15) and from (11) the amplifier input power $|A_s|^2$ can be found for operation at maximum added power. Not all values of gain are available and normally the limits of large signal $|s_a|$ are determined primarily by a solution to (13) for small signal s_r. Usually this small signal instability occurs at a different frequency than the operating frequency, as we shall show in Section V. The large signal equalization technique described above is now best illustrated by an example.

V. Application to Silicon Diodes and Realization of Optimum Efficiency Amplifiers

A. Quarter-Wavelength Equalization Networks

To verify the proposed technique of large signal equalization with conservation of maximum added power, we shall use a series of simple quarter-wavelength waveguide equalization networks at 37.5 GHz in conjunction with mounted silicon diodes characterized as described in Section III. The normalization at port 1 of these networks (Fig. 6) will be equal to that of port 2 which is considered the reference normalization (in this case 0.020×0.280 in). This required a broad-band waveguide transformer on the circulator port which was built into the circulator.

Under these conditions, a quarter-wavelength section of waveguide having a *relative height* h to the reference height (actual height/0.020 in) and the same waveguide width has s parameters given by

$$s_{11} = s_{22} = \frac{h^2 - 1}{h^2 + 1} \tag{16a}$$

and

$$s_{12} = -j \frac{2h}{h^2 + 1} . \tag{16b}$$

We have neglected any discontinuity capacitance occurring at the junction of the different size waveguides. Since s_{22} is real, then from Fig. 8 it is clear these sections are used most effectively if s_r is real at the quarter-wave frequency f_0. In practice $s_r(f_0)$ and in particular $s_{r0}(f_0)$ was made real by physically changing the reference plane (cutting of some waveguide), rotating s_r to the real axis.

TABLE I

A COMPARISON OF PREDICTED AND MEASURED PERFORMANCE FOR AN EQUALIZED IMPATT AMPLIFIER

h	s_{22}	$\frac{1}{\lvert s_a \rvert^{\dagger}}$	$\frac{1}{\lvert s_a \rvert^{*}}$	$P_i^{\dagger}$, mW	P_i^{*}, mW	P_{ga}^{*}, mW	$\lvert s_a \rvert^{2*}$ dP	P_o^{*}, mW
1	0.	.65	.65	150	150	205	3.74	355
1.1	.095	.592	.59	110	105	197	4.58	302
1.2	.180	.532	.52	81	74	200	5.68	274
1.3	.257	.472	.45	59	52	204	6.94	256

† Predicted from theory.
* Actual measured values.

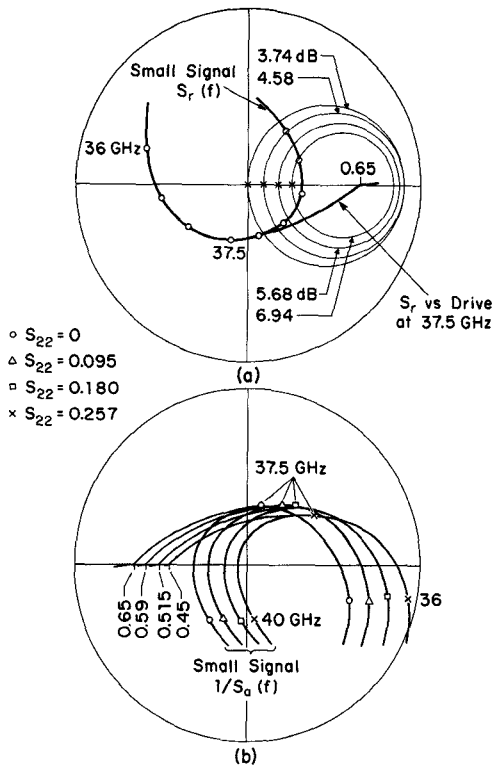

Fig. 9. (a) Small signal $s_r(f)$ and $s_r(P_{in})$ at 37.5 GHz. Crosses indicate gains predicted for the available quarter-wave equalization networks. (b) Equalized characteristics of (a) obtained with the addition of the quarter-wave networks.

B. Amplifier Performance

In Fig. 9(a) we have shown the small signal $s_r(f)$ and the large signal curve of $s_r(|A_d|^2)$ at 37.5 GHz for a mounted silicon diode with dc operating conditions of 5.1 W at 200 mA. The small signal curve will impose the limitations on the large signal gain through the stability requirement. For this diode, the maximum added power is 205 mW ($\eta_{dm} = 4$ percent) and occurs at the break in the large signal curve where $|A_{d0}|^2 = 150$ mW and $s_r = 0.65$ (3.74-dB gain). In order to make s_r real, we have physically modified the reference plane by shaving off some waveguide.

To demonstrate the large signal equalization technique in a simple effective manner, a series of quarter-wave sections at 37.5 GHz were fabricated which stepped in height from 0.020 to 0.030 in in steps of 0.001 in. The locus of $s_{22}(f)$ of these sections is a circle with a center at $s_{22,max}/2$ and radius $s_{22,max}/2$, where $s_{22,max}$ is given by (16a) and occurs at the quarter-wave frequency. Over the frequency range of interest, s_{22} changes little and it can be considered constant and equal to $s_{22,max}$ as given by (16a). Four different sections were used, and the corresponding values of s_{22} are indicated in Fig. 9(a) by the crosses on the real axis. Amplifier constant-gain circles are drawn which intersect these values of s_{22} and indicate the gain that is possible. A section of 0.028-in height was also tried but a weak oscillation at 39 GHz occurred as (13) was satisfied. The characteristics of $1/s_a$ resulting from this equalization are shown in Fig. 9(b), where again the small signal frequency behavior and large signal curve at 37.5 GHz are presented. The 180° phase shift is caused by the quarter-wave section. The maximum added power again occurs at the break point in the power curve when $1/s_a$ is approximately negative real as it should. The theoretical and experimental results of this equalization are compared in Table I. The disagreement between measured and predicted values for $|1/s_a|$ and input power P_i is thought to be caused by discontinuity capacitances at the steps in waveguide of the quarter-wave sections which were not considered in the calculations. Note that the added power, however, remains constant (to within measurement accuracy) as it does not depend on the gain as long as lossless equalization occurs. It is interesting to note from Fig. 9(b) that the maximum small signal gain occurs at about 39.1 GHz, or 1.6 GHz higher than the design frequency of 37.5 GHz. It is clear that any practice of "tuning" the circuit for high small signal gain at 37.5 GHz can severely limit the large signal amplifier capabilities at the same frequency. Finally, the limitation on large signal gain need not be caused by a small signal instability at 39.1 GHz as it was in this paper. By clever circuit design, it is entirely possible to have an $s_{22}(f)$ such that almost any large signal gain is achievable and (13) is not satisfied.

The power bandwidth available with these simple quarter-wave networks is as much as 5 GHz, or 13-percent fractional bandwidth. The reason for this can be observed from Fig. 10, where we have shown large signal curves at several frequencies along with the small signal $s_r(f)$ limit curve. The phase change at maximum added power is significantly less than at small signal and a quarter-wave network is effective over a wide bandwidth at large signal. To demonstrate this, a set of 7-dB gain circles are drawn at 36.5, 37.5, and 38.5 GHz and a

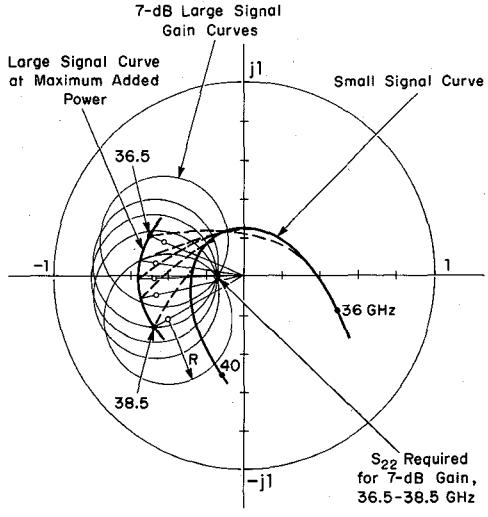

Fig. 10. Large and small signal s_r characteristics of a K_a-band mounted IMPATT demonstrating the bandwidth available at large signal.

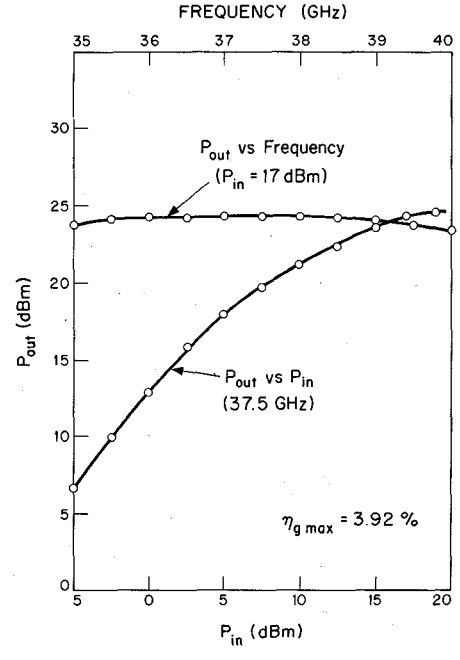

Fig. 11. Frequency response and P_o versus P_i for the equalized diode of Fig. 10.

matching section of $s_{22} = -0.15$ was chosen. The response of this amplifier is shown in Fig. 11, showing a 5-GHz 1-dB power bandwidth at 50-mW drive and 250-mW output. A single frequency P_i versus P_o curve is shown at 37.5 GHz. The generation efficiency of this amplifier is 3.94 percent at 5.1-W dc input. The physical realization of this amplifier is shown in Fig. 12.

C. Effects of Nonideal Circulators

A nonideal circulator modifies expected amplifier performance through its arm-to-arm insertion loss and nonzero input scattering coefficient s_c (Fig. 6). Normally for fractional bandwidths of 10 percent or less, the in-band performance of the circulator can be made to approach ideal, with insertion losses of 0.1 dB and return loss and isolation of greater than 20 dB. Usually the major problem encountered with nonideal

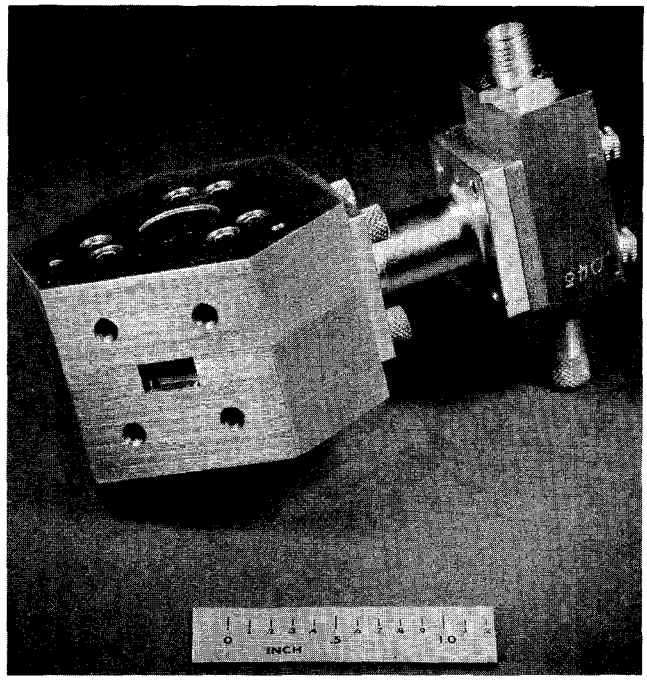

Fig. 12. Realization of the amplifier of Fig. 10.

circulators is an out-of-band instability since the gain bandwidth of the diode is often much larger than the effective circulation bandwidth. System stability under these conditions can be investigated by comparing either $1/s_a(f)$ to $s_c(f)$ or $s_r(f)$ to $s_0(f)$, where

$$s_0 = s_{22} + \frac{s_{12}^2}{\frac{1}{s_c} - s_{11}} \tag{17}$$

is the output scattering coefficient of the equalization network when the input is terminated in the circulator (s_c). In our design, plots of $s_0(f)$ and $s_r(f)$ were readily compared as $s_r(f)$ was available from previous characterization, and $s_0(f)$ could also be measured directly. The circulators used here were developed in conjunction with the amplifiers and typically had <0.1-dB insertion loss and >20-dB return loss and isolation over 35–38 GHz; instabilities could occur around 45 GHz at high bias currents.

VI. Summary and Conclusions

We have presented a procedure which is useful for design and realization of IMPATT-diode amplifiers which operate at maximum generation efficiency. The technique allows device characterization in a manner such that terminal conditions of a mounted diode can be identified that result in a maximum power exchange between the active network and a source. These terminal conditions are then used in conjunction with lossless equalization networks to design and realize optimum-efficiency stable amplifiers with a degree of gain flexibility. Although the procedure was effectively demonstrated using K_a-band silicon diodes in a waveguide environment, it should be applicable to most IMPATT diodes in their operating frequency range. In practice, it is felt this technique would allow a system containing IMPATT amplifiers to be designed optimally with respect to both gain and added power contribution per stage in a simple and effective manner.

ACKNOWLEDGMENT

The author wishes to thank D. M. Snider for helpful discussions, Prof. P. Penfield for allowing effective use of his circuit analysis program MARTHA, and C. Berglund for making many of the measurements.

REFERENCES

[1] W. J. Evans and G. I. Haddad, "A large signal analysis of IMPATT diodes," *IEEE Trans. Electron Devices*, vol. ED-15, pp. 708–717, Oct. 1968.
[2] M. Gilden and M. E. Hines, "Electronic tuning effects in the Read microwave avalanche diode," *IEEE Trans. Electron Devices (Special Issue on Semiconductor Bulk-Effect and Transit-Time Devices)*, vol. ED-13, pp. 169–175, Jan. 1966.
[3] W. T. Read, "A proposed high frequency negative resistance diode," *Bell Syst. Tech. J.*, vol. 37, pp. 401–466, Mar. 1968.
[4] H. K. Gummel and D. L. Scharfetter, "Avalanche region of IMPATT diodes," *Bell Syst. Tech. J.*, vol. 45, pp. 1797–1828, Dec. 1966.
[5] D. R. Decker, C. N. Dunn, and R. L. Frank, "Large-signal silicon and germanium avalanche-diode characteristics," *IEEE Trans. Microwave Theory Tech. (Special Issue on Microwave Circuit Aspects of Avalanche-Diode and Transferred Devices)*, vol. MTT-18, pp. 872–876, Nov. 1970.
[6] C. B. Swan, "IMPATT oscillator performance improvement with second harmonic tuning," *Proc. IEEE* (Lett.), vol. 56, pp. 1616–1617, Sept. 1968.
[7] C. A. Brackett, "Circuit effects in second-harmonic tuning of IMPATT diodes," *IEEE Trans. Electron Devices*, vol. ED-18, pp. 147–150, Mar. 1971.
[8] D. M. Snider, "A one-watt CW high-efficiency *X*-band avalanche-diode amplifier," *IEEE Trans. Microwave Theory Tech.* (Corresp.), vol. MTT-18, pp. 963–967, Nov. 1970.
[9] D. F. Peterson, "Characterization of an avalanche diode oscillator," M.S. thesis, Dep. Elec. Eng., Mass. Inst. Technol., Cambridge, Jan. 1969.
[10] W. E. Schroeder and G. I. Haddad, "Effect of harmonic and subharmonic signals on avalanche-diode oscillator performance," *IEEE Trans. Microwave Theory Tech.* (Corresp.), vol. MTT-18, pp. 327–331, June 1970.
[11] M. E. Hines, "Large signal noise, frequency conversion and parametric instabilities in IMPATT diode networks," to be published.
[12] D. H. Steinbrecher and D. F. Peterson, "Small-signal model with frequency-independent elements for the avalanche region of a microwave negative-resistance diode," *IEEE Trans. Electron Devices*, vol. ED-17, pp. 883–891, Oct. 1970.
[13] W. E. Schroeder, "Nonlinear properties of IMPATT diodes," Ph.D. dissertation, Univ. Michigan, Ann Arbor, 1972.

Large-Signal Equivalent Circuit for IMPATT-Diode Characterization and Its Application to Amplifiers

MADHU-SUDAN GUPTA

***Abstract*—A frequency-independent lumped equivalent circuit is proposed for characterizing the large-signal behavior of IMPATT diodes. It has five elements including a negative resistance, two of which are quadratic functions of the single-frequency RF voltage across the device. It is used for computer-aided analysis and the design of reflection-type negative-resistance amplifiers employing IMPATT diodes. The frequency response of the amplifier is calculated for different input power levels and the nature of the results is found to be in agreement with published experimental results.**

I. INTRODUCTION

A WEALTH of information is available in the literature on the design and analysis of reflection-type amplifiers, using negative-resistance devices such as tunnel diodes. The various techniques published can be classified into two groups depending upon the method used for characterization of the device. In one—the "time-domain method," the device is described by means of a time-domain i–v relationship $i=f(v)$ or $v=g(i)$, and given the instantaneous value of one of either v or i the other can be found. The function f (or g) is typically chosen as a cubic [1] or a power series [2]. This approach has been used extensively for tunnel-diode amplifier design and analysis. The method is not directly applicable to IMPATT diodes because their i–v relationship[1] is a nonlinear integro-differential equation which cannot be replaced by an instantaneous power-series relationship.

In the second method, which is the "frequency-domain method," the device is replaced by a nonlinear lumped impedance. This has also been used widely for tunnel-diode amplifier design [4]. Again, the results obtained for tunnel diodes cannot be extended to IMPATT diodes readily because, unlike tunnel diodes, the device impedance is not purely resistive, is a function of frequency over the operating range, and is nonlinear (signal dependent) under large-signal operating conditions.

Such characteristics of IMPATT diodes have severely limited the utility of many of the existing analyses of negative-resistance amplifiers and have necessitated the use of numerical methods. Further, the conventional computer-aided circuit-analysis programs are not sufficient for the analysis and design of amplifiers; they must be supplemented by numerical algorithms for solving carrier transport equations

Manuscript received March 5, 1973; revised May 4, 1973.
The author was with the Department of Electrical Engineering, Queen's University, Kingston, Ont., Canada. He is now with the Department of Electrical Engineering and the Research Laboratory of Electronics, Massachusetts Institute of Technology, Cambridge, Mass. 02139.

[1] For a sinusoidal voltage, the plot in the i–v plane shows a closed loop which depends upon signal amplitude and frequency [3].